IEEE Access
Multidisciplinary | Rapid Review | Open Access Journal

Received March 10, 2019, accepted March 24, 2019, date of publication April 1, 2019, date of current version April 15, 2019.

Digital Object Identifier 10.1109/ACCESS.2019.2908446

A Cost-Effective and Low-Complexity Predictive Control for Matrix Converters Under Unbalanced Grid Voltage Conditions

WENJING XIONG[1,2], YAO SUN[1,2], (Member, IEEE), JIANHENG LIN[1,2], MEI SU[1,2], HANBING DAN[1,2], MARCO RIVERA[3], (Senior Member, IEEE), AND JOSEP M. GUERRERO[4], (Fellow, IEEE)

[1]School of Automation, Central South University, Changsha 410083, China
[2]Hunan Provincial Key Laboratory of Power Electronics Equipment and Grid, Changsha 410083, China
[3]Faculty of Engineering, Universidad de Talca, Talca 2390123, Chile
[4]Department of Energy Technology, Aalborg University, 9220 Aalborg, Denmark

Corresponding author: Hanbing Dan (daniel698@sina.cn)

This work was supported in part by the National Key R&D Program of China under Grant 2018YFB0606005, in part by the National Natural Science Foundation of China under Grant 51807206, in part by the Key Technology R&D Program of Hunan Province of China under Grant 2018SK2140, in part by the Project of Innovation-Driven Plan in Central South University under Grant 2019CX003, and in part by the FONDECYT Research Project under Grant 1160690.

ABSTRACT Due to no dc-link energy storage element in the matrix converter (MC), its input and output performances are highly sensitive to the unbalanced grid conditions. In order to mitigate the adverse effects of the unbalanced grid voltages, this paper proposes a simple and effective control strategy based on the finite-control set model predictive control (FCS-MPC). In this case, an extended instantaneous power theory is adapted to generate the source current references. As a result, both sinusoidal source currents and balanced output currents are ensured. Besides, complicated positive and negative sequence decomposition is avoided. Furthermore, an extended state observer (ESO) is designed to eliminate the grid voltages sensors, which not only estimates the grid voltages but also provides the delayed grid voltage information required for the source current reference calculation. The effectiveness of the proposed method is verified by the simulation and experimental results.

INDEX TERMS Matrix converter, unbalanced gird voltages, extended state observer, finite-control set model predictive control.

I. INTRODUCTION

Matrix converter (MC) is a direct AC/AC converter, and it is featured by sinusoidal input and output currents, bidirectional energy flow, controllable input power factor and no dc-link component [1]–[3]. Due to the elimination of bulky and limited lifetime electrolytic capacitors, the reliability and power density of MC are higher than those of the conventional back-to-back converters [4]. Meanwhile, because of these characteristics, the voltage/current on input and output sides of MC are directly coupled. Then, all the inner variables, such as input and output currents, are easily influenced by extra disturbances.

The utility grid voltages would become unbalanced when considerable numbers of asymmetric loads are connected or short circuit faults occur. To suppress the adverse effects of unbalanced source voltages on the input and output performances of MC, many modulation strategies have been presented [5]–[19].

In [5]–[9], several space vector modulation (SVM) methods are introduced for MC/indirect MC (IMC) to improve the source current quality and balance the output currents. In [5], two SVM methods are presented. One is aligning the input current vector with the input voltage vector. Desired balanced output currents are obtained, but the source current contains a series of positive sequence harmonic components. The other can reduce or eliminate the harmonics of source currents by utilizing the information of positive and negative sequence components of source voltages. The modified SVM method in [7] can achieve balanced output currents, but the third-order harmonic component in source currents is relatively large. In [8], an online SVM method is introduced to optimize

The associate editor coordinating the review of this manuscript and approving it for publication was Huiqing Wen.

the duty cycles of the best switching states. To avoid the complex sequence component separation, a simple method for calculating the source current reference is proposed in [9]. Similar to the latter method in [5], a carrier-based modulation (CBM) strategy for IMC is presented in [10]. Additionally, based on the framework of SVM, some closed-loop control strategies are put forward [11]–[13]. To achieve balanced output currents and a near unity power factor (UPF) operation, an advanced closed-loop control for source currents is proposed for IMC [11]. In [12], two resonant controllers are adopted to regulate input currents and active power. Thus, the quality of input currents is improved without degrading the quality of output currents. In [13], a novel instantaneous effective power control method (IEPC) for MC under unbalanced grids is discussed.

Three enhanced double input line voltage synthesis (DLVS) methods are investigated in [14]–[15], they are aiming to achieve sinusoidal source currents. In [16], three mathematical construction methods are presented according to different ways of selecting the input current vector. These methods can achieve similar output current quality, but different input current quality. Three model predictive control (MPC) methods are proposed in [17], namely, active power oscillation compensation (APOC) strategy, the instantaneous unity power factor (IUPF) strategy and positive sequence (PS) strategy. Among these methods, the APOC strategy can achieve the best output and source current performance, but the calculation of source currents reference is complex. Literature [18] proposed an MPC method with reactive power minimization for IMC and literature [19] introduced a predictive current control method for MC. The quality of output currents is degraded with above two methods, as the ac-term in instantaneous active power cannot be completely eliminated.

Compared with SVM method, DLVS method, CBM method, and the mathematical construction method, the MPC method [20]–[24] appears as a promising alternative due to its simplicity and flexibility [3]. To reduce the complexity and improve the input/output performance of aforementioned methods, a cost-effective and low-complexity control method based on finite-control set MPC (FCS-MPC) is proposed for MC under unbalanced grid voltages in this study. The main ideas include 1) an extended instantaneous power theory for generating source current references is adopted to reduce the complexity of algorithm. 2) a non-static error extended state observer (ESO) based on internal model principle is proposed to reduce costs. With the new source current references, both the sinusoidal source currents and the balanced output currents are obtained. Besides, complicated positive and negative sequence decomposition is avoided. Because of the non-static error ESO, voltage sensors for grid voltages are saved. As the ESO also provides the delayed source voltages information, it does not increase total computational burden of the proposed method.

The remainder of this paper is organized as follows: Section II introduces the topology and the model of MC; in Section III, the proposed control scheme is described in detail; the simulation results of the proposed method and comparisons with other FCS-MPC-based strategies are provided in Section IV; in Section V, the experimental results are illustrated; and finally, the main points of this paper are summarized in Section VI.

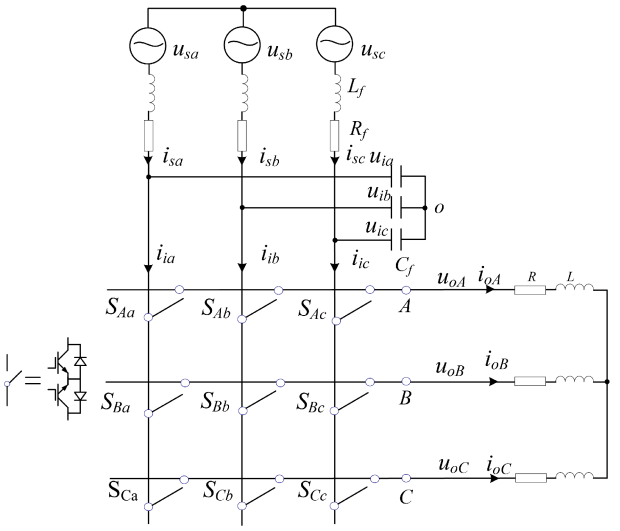

FIGURE 1. Topology of the matrix converter.

II. MC SYSTEM DESCRIPTION

A. TOPOLOGY OF MATRIX CONVERTER

The topology of MC is illustrated in Fig. 1. It mainly consists of the power grid interface, input LC filter, nine bidirectional switches, and three-phase balanced loads.

Assuming that the nine bidirectional switches are ideal, each switch $S_{yx}(x = a, b, c; y = A, B, C)$ has two possible states: $S_{yx} = 1$ when on state and $S_{yx} = 0$ when off-state. The states of nine switches can be represented as the following switching matrix

$$S = \begin{bmatrix} S_{Aa} & S_{Ab} & S_{Ac} \\ S_{Ba} & S_{Bb} & S_{Bc} \\ S_{Ca} & S_{Cb} & S_{Cc} \end{bmatrix} \tag{1}$$

For safety reasons, the input of MC cannot be short-circuited, and the output should not be left open due to the inductive loads. Thus, the switches should meet the following constraints

$$S_{ya} + S_{yb} + S_{yc} = 1, \quad y \in \{A, B, C\} \tag{2}$$

According to the constraints above, there are $3^3 = 27$ feasible switching states.

From Fig. 1, the relationship between the output and input voltages/currents are established as follows

$$\begin{bmatrix} u_{oA} \\ u_{oB} \\ u_{oC} \end{bmatrix} = \begin{bmatrix} S_{Aa} & S_{Ab} & S_{Ac} \\ S_{Ba} & S_{Bb} & S_{Bc} \\ S_{Ca} & S_{Cb} & S_{Cc} \end{bmatrix} \begin{bmatrix} u_{ia} \\ u_{ib} \\ u_{ic} \end{bmatrix} \tag{3}$$

$$\begin{bmatrix} i_{ia} \\ i_{ib} \\ i_{ic} \end{bmatrix} = \begin{bmatrix} S_{Aa} & S_{Ab} & S_{Ac} \\ S_{Ba} & S_{Bb} & S_{Bc} \\ S_{Ca} & S_{Cb} & S_{Cc} \end{bmatrix}^T \begin{bmatrix} i_{oA} \\ i_{oB} \\ i_{oC} \end{bmatrix} \tag{4}$$

where u_{ix} and u_{oy} represent the three phase input and output voltages, respectively, i_{ix} and i_{oy} represent the input and output currents, respectively.

B. MODELING OF MATRIX CONVERTER SYSTEM

The dynamic behavior of a general three-phase balanced load can be described as follows:

$$L\frac{d\vec{i}_o}{dt} = \vec{u}_o - R\vec{i}_o - \vec{e} \tag{5}$$

where L and R are the load inductance and resistance, respectively; $\vec{i}_o$ and $\vec{u}_o$ are the output current and voltage vector; $\vec{e}$ is the electromotive force (EMF) vector of the load. The load may cover *RL* load, induction motor, permanent magnet synchronous motor and grid. In this study, only the *RL* load is considered, thus $\vec{e} = 0$.

The continuous-time model of input side is described as the following equations:

$$\frac{d}{dt}\begin{bmatrix}\vec{u}_i\\ \vec{i}_s\end{bmatrix} = A\begin{bmatrix}\vec{u}_i\\ \vec{i}_s\end{bmatrix} + B\begin{bmatrix}\vec{u}_s\\ \vec{i}_i\end{bmatrix} \tag{6}$$

where

$$A = \begin{bmatrix}0 & 1/C_f\\ -1/L_f & -R_f/L_f\end{bmatrix}, B = \begin{bmatrix}0 & -1/C_f\\ 1/L_f & 0\end{bmatrix},$$

R_f, L_f, and C_f are the equivalent line resistance, the filter inductance and capacitance, respectively, $\vec{u}_s$ and $\vec{i}_s$ are the source voltage and current vectors, respectively, $\vec{u}_i$ and $\vec{i}_i$ are the input voltage and input current vectors.

III. PROPOSED CONTROL SCHEME

Usually, the control targets of MC under unbalanced grids are: 1) output voltages or currents regulation; 2) low-order harmonics reduction of the source currents with less contents and input reactive power control. To achieve these targets, a control method based on FCS-MPC is proposed for MC. Fig. 2 illustrates the overall control block diagram, which mainly involves an ESO and an MPC algorithm block. As shown, based on the novel power definition and the ESO, the source current reference is calculated. With the information of measured source currents and input voltages, the ESO can accurately estimate the source voltages and the delayed source voltages without using the grid voltage sensors, thus reducing the system costs. The MPC is an FCS-MPC, in which the sinusoidal source currents based on the novel power definition and balanced output currents are controlled. In this Section, the proposed control scheme will be introduced for MC in detail.

A. CALCULATION OF SOURCE CURRENT REFERENCE

Since there are no storage units in MC, the input instantaneous active power of MC is equal to its output instantaneous active power when the power losses are neglected. According to the first target, the input instantaneous active power of MC should keep constant. Regarding the second target, a certain reactive power will be regulated. However, the definition

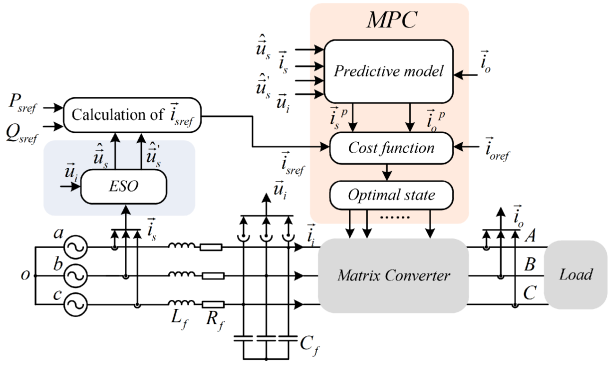

FIGURE 2. Block diagram of the proposed control scheme. (superscript 'p' denote as the predictive value at (k+2)-th instant).

of reactive power is non-unique [25]–[26]. For the same given active and reactive power, the obtained currents are different under different definitions of reactive power in the case of unbalanced voltages.

In this paper, the definitions of instantaneous active and reactive power based on the extension *pq* theory in [25] are introduced, where the input instantaneous active and reactive power of the MC can be expressed as

$$P_s = Re(\vec{i}_s^*\vec{u}_s) \tag{7}$$

$$Q_s = Re(\vec{i}_s^*\vec{u}_s^{'}) \tag{8}$$

where the superscript "$*$" denotes the conjugate of a vector; Re($\bullet$) is a function which extracts the real part from its argument. $\vec{u}_s^{'}$ denotes a vector whose phase lags $\vec{u}_s$ by 90 degrees.

As proved in [26], if Q_s is a constant, the oscillatory components in P_s can be eliminated naturally. That is, the definitions in (7) and (8) lay the foundation for the two control targets under unbalanced grids mentioned before.

Denote the unbalanced source voltage vector $\vec{u}_s$ as follows

$$\vec{u}_s(t) = U_P e^{j\omega t} + U_N e^{-j(\omega t-\varphi)} \tag{9}$$

where ω is the angular frequency of source voltages, U_P and U_N are the amplitude of positive and negative sequence voltage, respectively, while φ is the initial phase angle between positive and negative sequence voltage.

Then, the delayed source voltage $\vec{u}_s^{'}$ can be expressed as

$$\vec{u}_s^{'}(t) = -j(U_P e^{j\omega t} - U_N e^{-j(\omega t-\varphi)}) \tag{10}$$

Combine (7) $\sim$ (10), the source currents vector is solved as

$$\vec{i}_s = j\frac{P_s\vec{u}_s^{'}* - Q_s\vec{u}_s^*}{\mathrm{Im}(\vec{u}_s^{'*}\vec{u}_s)} \tag{11}$$

where Im($\bullet$) is a function which extracts the imaginary part from its argument, $\vec{x}^*$ represents the conjugate of $\vec{x}$.

The denominator $\mathrm{Im}(\vec{u}_s^{'*}\vec{u}_s) = \frac{3}{2}(U_P^2 - U_N^2)$ is a constant, $\vec{u}_s$ and $\vec{u}_s^{'}$ are sinusoidal. Thus, according to (11) when the constant active power P_s and reactive power Q_s are given, the sinusoidal source currents will be obtained under both balanced and unbalanced source voltages.

B. ESO FOR SOURCE VOLTAGES ESTIMATION

From(6), both the source voltages and input voltages have to be measured to implement the FCS-MPC. In order to reduce the costs, a non-static error ESO is proposed to estimate the source voltages.

Assume that the source voltages are unbalanced and its frequency is constant and known. Then, the model of the input side can be expressed as

$$\begin{cases} L_f \dfrac{di_{sx}}{dt} = u_{sx} - u_{ix} - R_f i_{sx} \\ \dfrac{du_{sx}}{dt} = -\omega u'_{sx} \\ \dfrac{du'_{sx}}{dt} = \omega u_{sx} \end{cases} \tag{12}$$

where i_{sx} and u_{sx} ($x = a,b,c$) are the source current and voltage, respectively, and u'_{sx} is the delayed source voltages.

Based on (12), a non-static error ESO is designed as

$$\begin{cases} L_f \dfrac{d\hat{i}_{sx}}{dt} = \hat{u}_{sx} - u_{ix} - R_f \hat{i}_{sx} + k_1 \left(i_{sx} - \hat{i}_{sx}\right) \\ \dfrac{d\hat{u}_{sx}}{dt} = -\omega \hat{u}'_{sx} + k_2 \left(i_{sx} - \hat{i}_{sx}\right) \\ \dfrac{d\hat{u}'_{sx}}{dt} = \omega \hat{u}_{sx} + k_3 \left(i_{sx} - \hat{i}_{sx}\right) \end{cases} \tag{13}$$

where k_1, k_2, and k_3 are coefficients, which will be determined later,$\hat{i}_{sx}$, $\hat{u}_{sx}$ and $\hat{u}'_{sx}$ are the estimated value of i_{sx}, u_{sx} and u'_{sx}, respectively.

Subtracting (12) from (13), we have

$$\frac{d}{dt}\begin{bmatrix} \tilde{i}_{sx} \\ \tilde{u}_{sx} \\ \tilde{u}'_{sx} \end{bmatrix} = A_E \begin{bmatrix} \tilde{i}_{sx} \\ \tilde{u}_{sx} \\ \tilde{u}'_{sx} \end{bmatrix} \tag{14}$$

where

$$A_E = \begin{bmatrix} -\left(R_f + k_1\right)/L_f & 1/L_f & 0 \\ -k_2 & 0 & -\omega \\ -k_3 & \omega & 0 \end{bmatrix},$$

and

$$\begin{bmatrix} \tilde{i}_{sx} \\ \tilde{u}_{sx} \\ \tilde{u}'_{sx} \end{bmatrix} = \begin{bmatrix} \hat{i}_{sx} - i_{sx} \\ \hat{u}_{sx} - u_{sx} \\ \hat{u}'_{sx} - u'_{sx} \end{bmatrix}$$

represents the estimation error.

Then, the characteristic equation of the proposed ESO is expressed as

$$\begin{aligned} \lambda(s) &= |sI - A_E| \\ &= s^3 + \frac{k_1 + R_f}{L_f} s^2 + \left(\frac{k_2}{L_f} + \omega^2\right) s + \frac{k_1 + R_f}{L_f}\omega^2 - \frac{k_3}{L_f}\omega \end{aligned} \tag{15}$$

To simplify the tuning process, all the poles are placed in the same location, then the desired λ(s) is formulated as

$$\lambda(s) = (s + \omega_c)^3 \tag{16}$$

where ω_c represents the location of the pole. Let (15) and (16) equal to each other, then k_1, k_2, and k_3 can be obtained accordingly.

$$\begin{cases} k_1 = 3\omega_c L_f - R_f \\ k_2 = \left(3\omega_c^2 - \omega^2\right) L_f \\ k_3 = \left(3\omega_c \omega - \omega_c^3/\omega\right) L_f \end{cases} \tag{17}$$

When $\omega_c > 0$, the designed A_E is a Hurwitz matrix. Then, the estimation error will be close to zero, and the convergence speed of the error is determined by ω_c.

On one hand, the grid voltages information are estimated by observer, which eliminates the voltage sensors and then reduces costs effectively. On the other hand, the delayed source voltage is also obtained by the observer. As a result, the extra strategy for obtaining the delayed source voltage is omitted, which reduces the computational burden to a certain extent.

C. DISCRETIZATION OF THE MC SYSTEM

To predict the future behavior of the system variables, the discrete-time model of MC should be developed. Assume that the control inputs are piecewise constant over the sampling period T_s, the model of input LC filter in (6) is discretized as follows,

$$\begin{bmatrix} \vec{u}_i^{k+1} \\ \vec{i}_s^{k+1} \end{bmatrix} = G \begin{bmatrix} \vec{u}_i^{k} \\ \vec{i}_s^{k} \end{bmatrix} + H \begin{bmatrix} \hat{\vec{u}}_s^{k} \\ \vec{i}_i^{k} \end{bmatrix} \tag{18}$$

where

$$G = e^{AT_s}, \quad H = A^{-1}(G - I)B \tag{19}$$

and the subscript 'k' and '$k+1$' denote as the k-th and $(k+1)$-th sampling time, respectively.

As the continuous-time models of the load and non-static error ESO in (5) and (13) can be written with the similar form of (18), so the discrete-time models of the load and ESO can also be obtained by (19).

D. CONSTRUCTION OF THE COST FUNCTION

The tasks of the FS-MPC are to track the desired input currents and output currents. Based on the discrete-time models and control objectives, the cost function can be constructed as follows.

1) CONTROL OF SOURCE CURRENTS

To achieve the sinusoidal source currents, the following cost function is constructed.

$$g_1 = \left\| \vec{i}_{sref} - \vec{i}_s^{k+2} \right\|^2 \tag{20}$$

where $\vec{i}_{sref}$ is the desired vector of source current, which can be obtained from (11) by replacing P_s and Q_s with P_{sref} and Q_{sref}; $\|\vec{x}\|$ denotes as the Euclidean norm of the vector $\vec{x}$.

To achieve the UPF operation, P_{sref} and Q_{sref} are given by

$$P_{sref} = P_{oref}/\eta, \quad Q_{sref} = 0 \tag{21}$$

where P_{oref} is the active power reference of load, which is determined by the type of loads, and η is the efficiency of the converter.

The active power reference P_{oref} of three phase balanced load can be written as

$$P_{oref} = \begin{cases} \frac{3}{2} I_{om}^2 R, & \text{when RL load} \\ T\Omega, & \text{when motor load} \\ \frac{3}{2} I_{om} U_{om} \cos\varphi_o. & \text{when grids} \end{cases} \tag{22}$$

where I_{om} is the amplitude of the output current reference, U_{om} is the amplitude of the voltage of balanced grid, φ_o is the desired displacement angle, T and Ω are the torque and angular speed reference of a motor, which can be obtained from the motor control.

As mentioned above, P_{sref} depends on two factors: η and P_{oref}. Although η is an unknown and time-varying parameter and P_{oref} is not accurately known, they have a little effect on the system performance. The imposed source currents by the instantaneous power can provide active damping for MC [29], [30]. And the reason for using the quantities at (k+2)-*th*sampling time in (20) is to compensate the time delay [18].

2) CONTROL OF OUTPUT CURRENTS

To achieve the desired output currents, the following cost function is considered.

$$g_2 = \left\| \vec{i}_{oref} - \vec{i}_o^{k+2} \right\|^2 \tag{23}$$

where $\vec{i}_{oref} = I_{om} \cos(\omega_o t - \varphi_o) + jI_{om} \sin(\omega_o t - \varphi_o)$ is the desired vector of output currents, ω_o is the angular frequency of output current.

The resulting cost function should reflect both the quality of source and output currents. Thus, the total cost function can be constructed as follows

$$F = g_2 + \lambda g_1 \tag{24}$$

To facilitate the adjustment of the weighting factor λ, the normalized total cost function is used.

$$\bar{F} = \frac{g_2}{\left\| \vec{i}_{oref} \right\|^2} + \lambda \frac{g_1}{\left\| \vec{i}_{sref} \right\|^2} \tag{25}$$

The weighting factor handles the relative importance of the two control objectives. Different choices of weighting factor lead to different comprehensive performance. Usually, the weighting factor selected by trial and error method [31].

E. IMPLEMENTATION PROCESS

The implementation process of the proposed method is shown in Fig. 3.

Step 1: Measure the source current $\vec{i}_s^k$, input voltage $\vec{u}_i^k$ and output current $\vec{i}_o^k$, and estimate the source voltages $\hat{\vec{u}}_s^k$ and $\hat{\vec{u}}_s' k$.

Step 2: Calculate the reference signals $\vec{i}_{sref}$ and $\vec{i}_{oref}$ by (11) and (23).

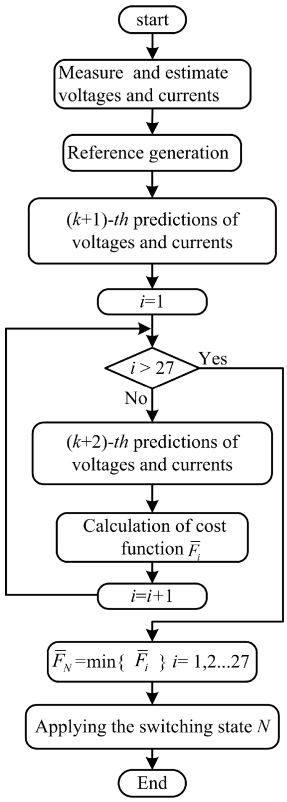

FIGURE 3. Flowchart of the proposed FCS-MPC method.

Step 3: Calculate the output voltage $\vec{u}_o^k$ and input current $\vec{i}_i^k$ by (3), (4) and the current switching state S^k, and then predict the voltages and currents at the $(k+1)$-th sampling period by combining (5), (6) and (19), include $\vec{i}_s^{k+1}$, $\hat{\vec{u}}_s^{k+1}$, $\hat{\vec{u}}_s' k+1$, $\vec{u}_i^{k+1}$, and $\vec{i}_o^{k+1}$.

Step 4: Repeat step 3 for all the 27 valid switching states to predict the voltages and currents at the $(k+2)$-th sampling period.

Step 5: Evaluate the cost function (25) and apply the optimal switching state at the $(k+1)$-th sampling period.

Then, repeat all the steps in the next switching time.

IV. SIMULATION RESULTS

In this Section, simulations have been carried out on MC system to illustrate and validate the proposed method. Besides, the comparisons with other FCS-MPC methods for unbalanced grids are given.

A. SIMULATIONS OF PROPOSED METHOD

Numerical simulations are carried out in Matlab/Simulink platform. The related parameters are listed in Table 1.

The proposed ESO, in which ω_c is set to 1000π rad/s, is tested under unbalanced source voltages ($U_{sa} = U_{sb} = 60$V, $U_{sc} = 40$V). The waveforms of the estimated voltage $\hat{u}_{sa}$, delayed voltage $\hat{u}_{sa}'$ and estimated error $\tilde{u}_{sa}$ are shown in Fig. 4. As seen, the estimated error is almost zero, $\hat{u}_{sa}'$ has the same amplitude with $\hat{u}_{sa}$, and $\hat{u}_{sa}'$ lags $\hat{u}_{sa}$ 90 degrees, which proves the feasibility of the ESO.

TABLE 1. Parameters of the matrix converter system.

Parameters	Value
Source voltage frequency(f_i)	50 Hz
Control period (T_s)	100 μs
Input mains and filter inductor (L_f)	0.6 mH
Input filter capacitor (C_f)	66 μF
Input passive damping resistor (R_f)	0.02 Ω
Resistor of load (R)	5.5 Ω
Inductor of load (L)	6 mH
Weighting factor (λ)	1.0

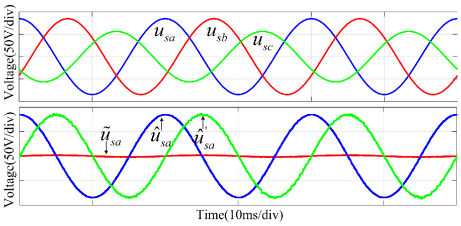

FIGURE 4. Waveforms of the unbalanced source voltages and the estimated voltages by ESO.

When the amplitude and frequency of reference output currents are set to 10A and 30Hz, respectively. The simulation results under proposed method are shown in Fig. 5(a). From top to bottom, they are source current i_{sa} and source voltage u_{sa}, source currents i_{sa}, i_{sb}, i_{sc}, and output currents i_{oA}, i_{oB}, i_{oC}. As seen, the source currents are basically sinusoidal, the output currents are balanced, and almost UPF is achieved.

B. SIMULATION COMPARISONS

The comparisons are performed among the following four FCS-MPC methods: the proposed method, PS strategy [17], IUPF strategy [17], [18], and APOC method [17].

In IUPF strategy, the source current reference is calculated by making the conventional instantaneous power a constant. The balanced output currents can be achieved, but the quality of input current cannot be assured. In PS strategy, the positive sequence component of source voltages is adopted to generate the source current reference. The balanced source currents could be obtained. However, the quality of output currents is poor as the ac-term in output active power will exists inevitably in this case. In APOC strategy, sinusoidal source currents and balanced output currents could be achieved simultaneously. The proposed method and APOC are equivalent in input-output characteristics. The difference between them lies in the methods to calculate the source current reference, which will be reflected in computational burden.

The simulation results of above methods are shown in Fig. 5. The uniform cost function (25) is adopted and the weighting factor of four methods is set to 1.0. The simulation

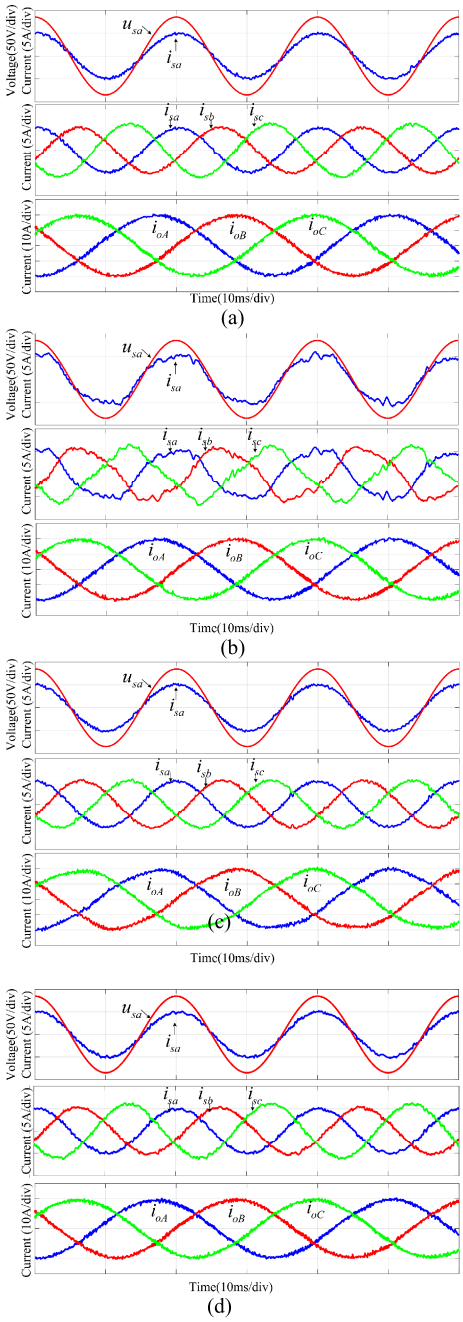

FIGURE 5. Simulation results of three different FCS-MPC methods. (a) Proposed method. (b) IUPF strategy. (c) PS strategy. (d) APOC strategy.

results of IUPF strategy is shown in Fig. 5(b), the balanced output currents can be achieved but the source currents are distorted seriously. The waveforms of PS strategy are illustrated in Fig. 5(c). The balanced source and output currents and almost UPF operation are achieved. Seen from Fig. 5(a) and Fig. 5(d), the APOC strategy and the proposed method are basically the same, the sinusoidal source currents and balanced output currents are achieved.

The total harmonic distortions (THDs) of source currents and output currents under the above methods are listed in Table 2. As demonstrated, the current quality under the

TABLE 2. THDs of source and output simulation waveforms under different FCS-MPC methods.

Method	THD of source currents			THD of output currents		
	i_{sa}	i_{sb}	i_{sc}	i_{oA}	i_{oB}	i_{oC}
IUPF	13.22%	12.98%	13.3%	3.71%	3.64%	3.75%
PS	5.42%	5.25%	5.54%	4.75%	4.70%	4.72%
APOC	4.80%	4.74%	4.39%	3.68%	3.64%	3.62%
Proposed method	4.80%	4.74%	4.39%	3.68%	3.64%	3.62%

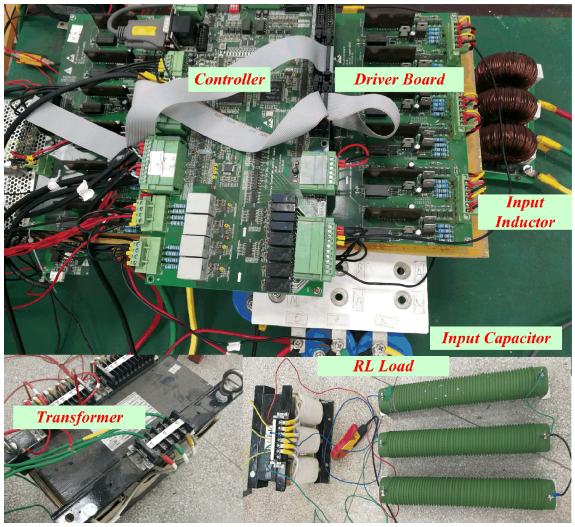

FIGURE 6. Experimental setup.

proposed method and the APOC strategy are the same and they have the best current quality, the quality of output currents under PS strategy is the worst, and the quality of source currents under IUPF strategy is the worst.

V. EXPERIMENTAL RESULTS

To validate the proposed control scheme, experiments have been carried out on the MC system. The experimental setup is shown in Fig. 6, which includes transformer, main circuit, input LC filter, controller board, drive boards, clamp circuit, and a three-phase balanced *RL*load. The main circuit consists of nine bi-directional switches, which are realized by the IGBT module FF200R12KT3_E. The main controller mainly includes: a floating-point digital signal processor (DSP) TMS320F28335 and a field programmable gate array (FPGA) EP2C8J144C8N. The DSP is responsible for implementing the proposed method and transmitting the optimal switching states to FPGA. The FPGA is used to generate the PWM signals to the drive boards. The related experimental parameters are the same with the parameters as listed in Table 1.

The experiments are carried out in the following cases:

Case I : the source voltages are balanced, and $U_{\rm sa} = U_{\rm sb} = U_{\rm sc} = 60$V (RMS);

Case II: the source voltages are unbalanced, and $U_{\rm sa} = U_{\rm sb} = 60$V, $U_{\rm sc} = 40$V.

Case III: the source voltages are seriously unbalanced, and $U_{\rm sa} = U_{\rm sb} = 60$V, $U_{\rm sc} = 120$V.

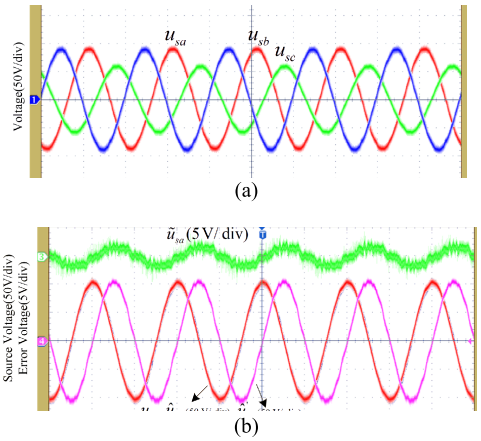

FIGURE 7. Unbalanced source voltages.

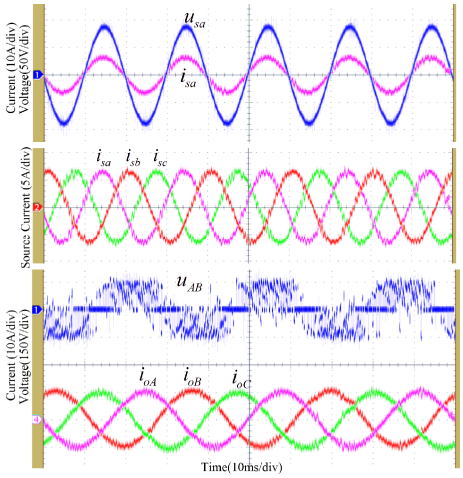

FIGURE 8. Input and output waveforms under case I.

A. EXPERIMENTS OF PROPOSED METHOD

First, the feasibility of designed ESO is tested. By FFT analysis, the THDs of source voltages under case II are 3.37%, 3.58% and 4.95%. The voltages u_{sa}, $\hat{u}_{sa}$, $\hat{u}'_{sa}$ and $\tilde{u}_{sa}$ are shown in Fig. 7(b), u_{sa} and $\hat{u}_{sa}$ are coincident, and the estimated error is small and within $\pm$3V. As a conclusion, the designed ESO can track the source voltages well even though there exist some harmonics in the source voltages.

In case I, when the amplitude and frequency of output current are set to 10A and 30Hz respectively, the measured input and output waveforms are shown in Fig. 8. As seen, the source currents and output currents are balanced. Additionally, the UPF operation is achieved.

In case II, two different reference output currents are tested: $f_o = 30$Hz, $I_{om} = 10$A and $f_o = 60$Hz, $I_{om} = 10$A. The power reference and amplitude of output current reference are the same under the two conditions, so the source currents will be the same. The waveforms of source currents and calculated power are illustrated in Fig. 9, where the instantaneous power is calculated by DSP, and attenuated by 200 times, then output to the oscilloscope through the D/A converter chip AD5725. The source currents are basically sinusoidal but unbalanced,

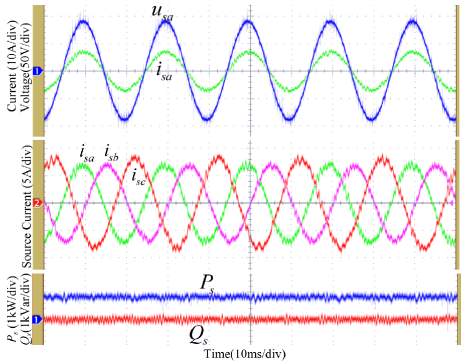

FIGURE 9. Input waveforms of the proposed method under case II.

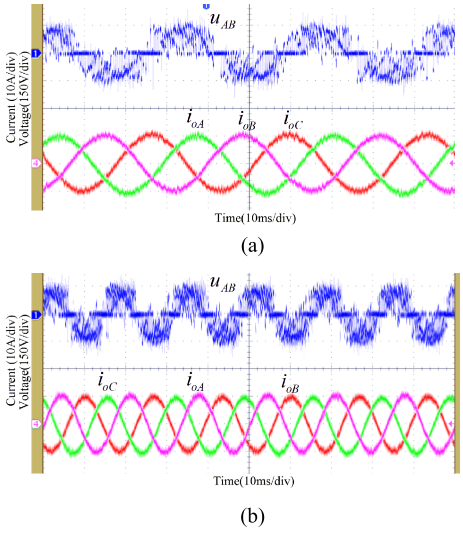

FIGURE 10. Output waveforms of the proposed method under case II. (a) $f_o = 30$Hz, $I_{om} = 10$A; (b) $f_o = 60$Hz, $I_{om} = 10$A.

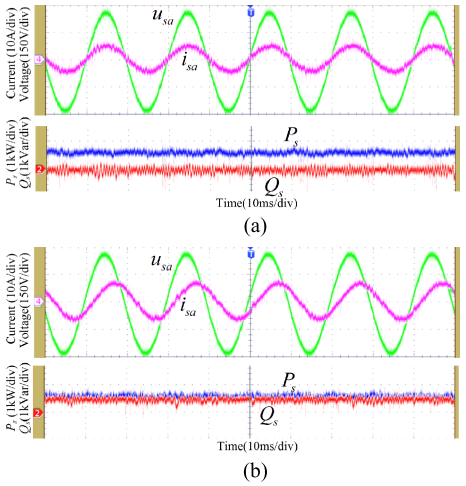

FIGURE 11. Waveforms with different reactive power settings under case II ($f_o = 30$Hz, $I_{om} = 6$A). (a) $Q_{sref} = 0$Var; (b) $Q_{sref} = 400$Var.

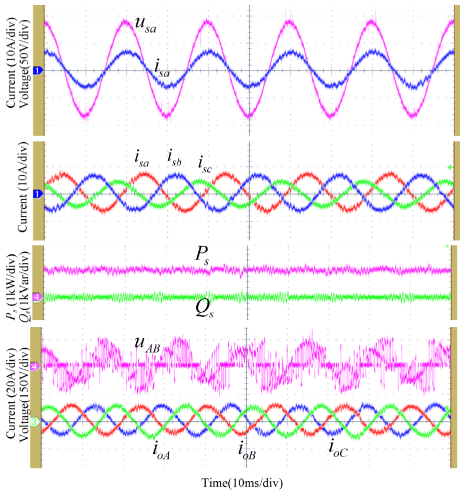

FIGURE 12. Experimental waveforms of the proposed method under case III ($f_o = 60$Hz, $I_{om} = 11A$).

P_s and Q_s are controlled to be constant values without double-frequency ripple power. The phase shift between source voltage u_{sa} and source current i_{sa} is almost zero, but the conclusion that the system operates at UPF cannot be drawn. The reasons is that the phase-shift of each source current in Fig. 9 is not 120 degrees. In fact, Q_s equals to zero represents that the sum of reactive powers of three input phases is zero, rather than that the source current is in phase with the respective source voltage. Fig. 10 shows the waveforms of output phase-to-phase voltage and output currents, the output currents under different conditions are balanced. Besides, it can be observed from Fig. 10(a) and Fig. 8 that the output currents are basically the same. It can be concluded that the balanced output currents, constant instantaneous active power and minimum instantaneous reactive power can be achieved under unbalanced input voltages regardless of the output frequency, which verifies the effectiveness of the proposed method.

Further, different reactive power references are performed by the proposed method under case II. In Fig. 11(a) and Fig. 11(b), the output currents are set to 6A/30Hz, Q_{sref} are set to 0Var and 400Var respectively. As seen, the calculated power are controlled to be constant values under two conditions, which means the source currents are sinusoidal and the output currents are balanced. In addition, there is an apparent phase shift between u_{sa} and i_{sa} when $Q_{sref} = 400$Var. It can be concluded that the proposed method has the capability to control the reactive power under the premise of ensuring the quality of source and output currents.

Fig. 12 shows the waveforms in case III with $f_o = 60$Hz, $I_{om} = 11$A. As seen, the source currents are basically sinusoidal and the output currents are balanced, P_s and Q_s are constant, which confirm the effectiveness of the proposed method again.

In addition, a series of experiments are tested to show the effects of efficiency settings on system performance under case III with $f_o = 60$Hz, $I_{om} = 11$A. The measured values of source currents and output currents under different efficiency settings are listed in Table 3. It is observed that the differences

TABLE 3. Amplitude and THD Of source currents and output currents with different efficiency values.

η	Amplitude and THD of source currents			Amplitude and THD of output currents		
	i_{sa}	i_{sb}	i_{sc}	i_{oA}	i_{oB}	i_{oC}
0.8	8.253A/ 7.72%	7.587A/ 7.87%	5.4A/ 9.21%	11.03A/ 7.37%	11A/ 7.11%	11.02A/ 7.23%
0.85	8.118A/ 7.4%	7.453A/ 7.65%	5.314A/ 8.94%	10.91A/ 7.12%	10.92A/ 7.03%	10.94A/ 7.0%
0.90	8.001A/ 7.27%	7.334A/ 7.46%	5.253A/ 8.79%	10.88A/ 6.86%	10.85A/ 6.96%	10.85A/ 6.93%
0.95	7.827A/ 7.17%	7.166A/ 7.32%	5.108A/ 8.6%	10.71A/ 6.80%	10.72A/ 7.19%	10.71A/ 6.82%

TABLE 4. THDs of source and output experimental waveforms under different FCS-MPC methods.

Method	THD of source currents			THD of output currents		
	i_{sa}	i_{sb}	i_{sc}	i_{oA}	i_{oB}	i_{oC}
IUPF	15.04%	15.6%	16.42%	7.5%	7.36%	7.32%
PS	8.29%	8.49%	8.08%	8.95%	8.36%	8.27%
APOC	7.68%	7.54%	7.28%	6.76%	6.59%	6.60%
Proposed Method	7.54%	7.57%	7.26%	6.62%	6.68%	6.63%

of source current amplitude and output current amplitude are not significant when the efficiency derivation over a large interval. The THD of output currents are quite close under different efficiency settings. As a conclusion, the efficiency setting η has little effect on the quality of source and output currents.

B. EXPERIMENTAL COMPARISONS

For comparison purpose, the waveforms of IUPF strategy, PS strategy and APOC strategy under case II with $f_o = 30$Hz, $I_{om} = 10$A are shown in Fig. 13(a), Fig. 13(b) and Fig.13(c), respectively. From top to bottom, they are source current i_{sa} and source voltage u_{sa}, source currents i_{sa}, i_{sb}, i_{sc}, conventional instantaneous power P_s and $Q_c(Q_c = \mathrm{Im}(\vec{i}_s^* \vec{u}_s))$, output phase-to-phase voltage u_{AB} and output currents i_{oA}, i_{oB}, i_{oC}. As illustrated in Fig. 13(a), the output currents are balanced but the source currents are distorted under IUPF strategy. In addition, P_s and Q_c are controlled to be constant values, which means that the source currents' quality are sacrificed to assure the output currents' quality. In Fig. 13(b), the balanced source currents are also obtained, but the instantaneous active power and reactive power are fluctuant, so the output current quality is relatively poor. Comparing Fig. 13(c) with Fig. 9 and Fig. 10 (a), the source currents and output currents of the APOC strategy and the proposed method are basically the same. A clear distinction is that Q_s is constant but Q_c is fluctuant.

To evaluate the harmonic performance of four FCS-MPC methods in an intuitive way, the THDs of the source and output currents under case II are illustrated in Table 4. As demonstrated, the current quality of APOC strategy and the proposed method are basically the same and superior to IUPF strategy and PS strategy, which is in accordance with the simulation results in Section IV (Table 2).

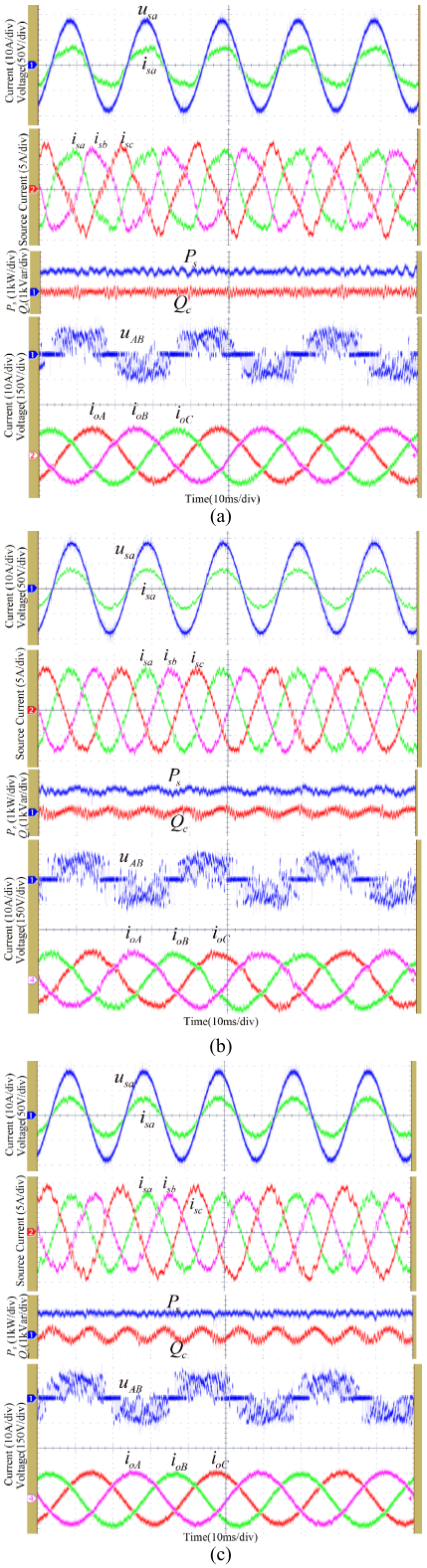

FIGURE 13. Experimental waveforms of different FCS-MPC methods under case II ($f_o = 30$Hz, $I_{om} = 10$A). (a) IUPF strategy (b) PS strategy (c) APOC strategy.

The execution time required by the mentioned four FCS-MPC methods are listed in Table 5. The required execution time for IUPF strategy is the least, because its source

TABLE 5. Execution time of different FCS-MPC methods.

Method	Execution time (μs)					
	ESO	A/D	Reference Calculation	Prediction &Evaluation	Other Algorithms	Total
IUPF	/	2.2	1.6	67.7	1.4	72.9
PS	/	2.2	2.4	67.7	1.4	73.7
APOC	/	2.2	4.0	67.7	1.4	75.3
Proposed Method	0.8	1.5	1.6	67.7	1.4	73.0

current reference is calculated by the source voltages and expected power directly. As the positive sequence component of source voltages needs to be extracted, the PS strategy takes slightly longer execution time. It worth noting that IUPF strategy and PS strategy need less computation time, but their input and output performance are poor. The APOC strategy has the excellent input and output current quality, but it takes the longest execution time. The reason is that both the positive and negative sequence component of source voltages are needed. The reference calculation process of the proposed method is very simple. Thus, the total execution time for the proposed method is short even though an ESO is added. As a conclusion, the proposed method can achieve good input and output current performance, save the system cost and reduce the computational time.

VI. CONCLUSION

In this paper, a predictive control based on new reactive power definition is presented for matrix converter under unbalanced source voltage conditions. Under this control scheme, the ac-term in active power could be eliminated, together with balanced output currents and sinusoidal source currents. Moreover, the grid voltage sensors are no longer needed and the phase-locked loop and positive/negative sequence decomposition are not required, resulting in the reduction of system costs and computational burdens. In fact, it is a general control strategy for MC under both balanced and unbalanced source voltage conditions. These characteristics make this strategy more suitable for practical applications.

Furthermore, the proposed method can be extended to other converters (e.g. three-phase voltage source rectifier and three-phase current source rectifier) to improve the input or output performance and reduce the system costs under unbalanced input conditions.

REFERENCES

[1] P. W. Wheeler, J. Rodriguez, J. C. Clare, L. Empringham, and A. Weinstein, "Matrix converters: A technology review," *IEEE Trans. Ind. Electron.*, vol. 49, no. 2, pp. 276–288, Apr. 2002.
[2] D. Casadei, G. Serra, A. Tani, and L. Zarri, "Matrix converter modulation strategies: A new general approach based on space-vector representation of the switch state," *IEEE Trans. Ind. Electron.*, vol. 49, no. 2, pp. 370–381, Apr. 2002.
[3] J. Rodríguez, M. Rivera, J. W. Kolar, and P. W. Wheeler, "A review of control and modulation methods for matrix converters," *IEEE Trans. Ind. Electron.*, vol. 59, no. 1, pp. 58–70, Jan. 2012.
[4] P. Zanchetta, P. Wheeler, L. Empringham, and J. Clare, "Design control and implementation of a three-phase utility power supply based on the matrix converter," *IET Power Electron.*, vol. 2, no. 2, pp. 156–162, Mar. 2009.
[5] D. Casadei, G. Serra, and A. Tani, "Reduction of the input current harmonic content in matrix converters under input/output unbalance," *IEEE Trans. Ind. Electron.*, vol. 45, no. 3, pp. 401–411, Jun. 1998.
[6] F. Blaabjerg, D. Casadei, C. Klumpner, and M. Matteini, "Comparison of two current modulation strategies for matrix converters under unbalanced input voltage conditions," *IEEE Trans. Ind. Electron.*, vol. 49, no. 2, pp. 289–296, Apr. 2002.
[7] X. Wang, H. Lin, H. She, and B. Feng, "A research on space vector modulation strategy for matrix converter under abnormal input-voltage conditions," *IEEE Trans. Ind. Electron.*, vol. 59, no. 1, pp. 93–104, Jan. 2012.
[8] J. D. Dasika and M. Saeedifard, "An online modulation strategy to control the matrix converter under unbalanced input conditions," *IEEE Trans. Power Electron.*, vol. 30, no. 8, pp. 4423–4436, Aug. 2015.
[9] J. Lei, B. Zhou, J. Bian, X. Qin, and J. Wei, "A simple method for sinusoidal input currents of matrix converter under unbalanced input voltages," *IEEE Trans. Power Electron.*, vol. 31, no. 1, pp. 21–25, Jan. 2016.
[10] X. Liu, F. Blaabjerg, P. C. Loh, and P. Wang, "Carrier-based modulation strategy and its implementation for indirect matrix converter under unbalanced grid voltage conditions," in *Proc. Conf. EPE/PEMC*, Novi Sad, Serbia, Sep. 2012, pp. LS6a.2-1–LS6a.2-7.
[11] M. Hamouda, H. F. Blanchette, and K. Al-Haddad, "Unity power factor operation of indirect matrix converter tied to unbalanced grid," *IEEE Trans. Power Electron.*, vol. 31, no. 2, pp. 1095–1107, Feb. 2016.
[12] J. Lei *et al.*, "Feedback control strategy to eliminate the input current harmonics of matrix converter under unbalanced input voltages," *IEEE Trans. Power Electron.*, vol. 32, no. 1, pp. 878–888, Jan. 2017.
[13] I. Sato, J.-I. Itoh, H. Ohguchi, A. Odaka, and H. Mine, "An improvement method of matrix converter drives under input voltage disturbances," *IEEE Trans. Power Electron.*, vol. 22, no. 1, pp. 132–138, Jan. 2007.
[14] J.-K. Kang, H. Hara, A. M. Hava, E. Yamamoto, E. Watanabe, and T. Kume, "The matrix converter drive performance under abnormal input voltage conditions," *IEEE Trans. Power Electron.*, vol. 17, no. 5, pp. 721–730, Sep. 2002.
[15] Y. Yan, H. An, T. Shi, and C. Xia, "Improved double line voltage synthesis of matrix converter for input current enhancement under unbalanced power supply," *Power Electron., IET*, vol. 6, no. 4, pp. 798–808, Apr. 2013.
[16] X. Li, M. Su, Y. Sun, H. Dan, and W. Xiong, "Modulation strategies based on mathematical construction method for matrix converter under unbalanced input voltages," *IET Power Electron.*, vol. 6, no. 3, pp. 434–445, Mar. 2013.
[17] C. Rojas *et al.*, "Predictive control of a direct matrix converter operating under an unbalanced AC source," in *Proc. IEEE ISIE*, Bari, Italy, Jul. 2010, pp. 3159–3164.
[18] M. Rivera, J. Rodríguez, J. R. Espinoza, and H. Abu-Rub, "Instantaneous reactive power minimization and current control for an indirect matrix converter under a distorted AC supply," *IEEE Trans. Ind. Informat.*, vol. 8, no. 3, pp. 482–490, Aug. 2012.
[19] T.-L. Nguyen and H.-H. Lee, "A predictive current control for coordinate control of current and power of matrix converter under unbalanced input voltages," in *Proc. ICMWT*, Kuala Lumpur, Malaysia, Jun. 2017, pp. 528–538.
[20] S. Muller, U. Ammann, and S. Rees, "New time-discrete modulation scheme for matrix converters," *IEEE Trans. Ind. Electron.*, vol. 52, no. 6, pp. 1607–1615, Dec. 2005.
[21] M. Siami, D. A. Khaburi, M. Rivera, and J. Rodríguez, "An experimental evaluation of predictive current control and predictive torque control for a PMSM fed by a matrix converter," *IEEE Trans. Ind. Electron.*, vol. 64, no. 11, pp. 8459–8471, Nov. 2017.
[22] R. Vargas, U. Ammann, J. Rodriguez, and J. Pontt, "Predictive strategy to control common-mode voltage in loads fed by matrix converters," *IEEE Trans. Ind. Electron.*, vol. 55, no. 12, pp. 4372–4380, Dec. 2008.
[23] R. Vargas, U. Ammann, and J. Rodríguez, "Predictive approach to increase efficiency and reduce switching losses on matrix converters," *IEEE Trans. Power Electron.*, vol. 24, no. 4, pp. 894–902, Apr. 2009.
[24] T. Peng *et al.*, "Open-switch fault diagnosis and fault tolerant for matrix converter with finite control set-model predictive control," *IEEE Trans. Ind. Electron.*, vol. 63, no. 9, pp. 5953–5963, Sep. 2016.
[25] Y. Komatsu and T. Kawabata, "A control method of active power filter in unsymmetrical and distorted voltage system," in *Proc. Conf. EPE*, Sevilla, Spain, Sep. 1995, pp. 904–907.
[26] Y. Suh and T. A. Lipo, "Modeling and analysis of instantaneous active and reactive power for PWM AC/DC converter under generalized unbalanced network," *IEEE Trans. Power Del.*, vol. 21, no. 3, pp. 1530–1540, Jul. 2006.

[27] Y. Zhang and C. Qu, "Model predictive direct power control of PWM rectifiers under unbalanced network conditions," *IEEE Trans. Ind. Electron.*, vol. 62, no. 7, pp. 4011–4022, Jul. 2015.
[28] Y. Zhang, J. Liu, H. Yang, and J. Gao, "Direct power control of pulsewidth modulated rectifiers without DC voltage oscillations under unbalanced grid conditions," *IEEE Trans. Ind. Electron.*, vol. 65, no. 10, pp. 7900–7910, Oct. 2018.
[29] M. Rivera *et al.*, "Imposed sinusoidal source and load currents for an indirect matrix converter," *IEEE Trans. Ind. Electron.*, vol. 59, no. 9, pp. 3427–3435, Sep. 2012.
[30] M. Rivera, C. Rojas, J. Rodriguez, and J. Espinoza, "Methods of source current reference generation for predictive control in a direct matrix converter," *IET Power Electron.*, vol. 6, no. 5, pp. 894–901, 2013.
[31] P. Cortes *et al.*, "Guidelines for weighting factors design in model predictive control of power converters and drives," in *Proc. IEEE ICIT*, Gippsland, VIC, Australia, Feb. 2009, pp. 1–7.

WENJING XIONG was born in Hunan, China, in 1991. She received the B.S. degree in automation and the Ph.D. degree in control science and engineering from Central South University, Changsha, China, in 2012 and 2017, respectively, where she is currently a Lecturer with the School of Automation.

Her research interests include matrix converter and ac/dc converter.

YAO SUN (M'13) was born in Hunan, China, in 1981. He received the B.S., M.S., and Ph.D. degrees from the School of Information Science and Engineering, Central South University, Changsha, China, in 2004, 2007, and 2010, respectively, where he has been a Professor with the School of Automation.

His research interests include matrix converter, and micro-grid and wind energy conversion systems.

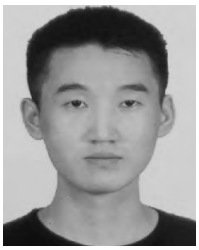

JIANHENG LIN was born in Fujian, China, in 1994. He received the B.S. degree in electronic engineering from Jimei University, Xiamen, China, in 2016. He is currently pursuing the Ph.D. degree in control science and engineering with Central South University, Changsha.

His research interests include linear time periodic system analysis, and matrix converter.

MEI SU was born in Hunan, China, in 1967. She received the B.S. degree in automation, and the M.S. and Ph.D. degrees in electric engineering from the School of Information Science and Engineering, Central South University, in 1989, 1992, and 2005, respectively, where she has been a Professor, since 2005. She is currently an Associate Dean of the School of Automation, Central South University.

Her research interests include matrix converter, adjustable-speed drives, and wind energy conversion systems. She is currently an Associate Editor of the IEEE TRANSACTIONS ON POWER ELECTRONICS.

HANBING DAN was born in Hubei, China, in 1991. He received the B.S. degree in automation and the Ph.D. degree in control science and engineering from Central South University, Changsha, China, in 2012, and 2017, respectively.

He was a Visiting Researcher with the Faculty of Engineering, University of Nottingham, U.K., from 2016 to 2017. He is currently an Associate Professor with the School of Automation, Central South University, China. His research interests include matrix converter, finite control set-model predictive control, motor control, fault diagnosis and fault tolerant of power converter, and wireless power transfer.

MARCO RIVERA (S'09–M'11–SM'17) received the B.Sc. degree in electronics engineering and the M.Sc. degree in electrical engineering from the Universidad de Concepcion, Chile, in 2007 and 2008, respectively, and the Ph.D. degree from the Department of Electronics Engineering, Universidad Tecnica Federico Santa Maria, Valparaíso, Chile, in 2011, with a scholarship from the Chilean Research Fund CONICYT.

From 2011 to 2012, he held a postdoctoral position and was a part-time Professor of digital signal processors and industrial electronics with Universidad Tecnica Federico Santa Maria. He is currently an Associate Professor with the Faculty of Engineering, Universidad de Talca, Curicó, Chile. His research interests include matrix converters, predictive and digital controls for high-power drives, four-leg converters, renewable energies, and development of high-performance control platforms based on field-programmable gate arrays.

Dr. Rivera is a member of the Advisory Council of the Civil Society for the Ministry of Energy. He received a scholarship from the Marie Curie Host Fellowships for early stage research training in electrical energy conversion and conditioning technology at the University College Cork, Cork, Ireland, in 2008. In 2012, he received the Chilean Academy of Science Doctoral Thesis Award (Premio Tesis de Doctorado Academia Chilena de Ciencias) for the Best Ph.D. Thesis published, in 2011, selected from among all national and international students enrolled in any exact or natural sciences program in Chile, and the Outstanding Engineer, in 2015.

JOSEP M. GUERRERO (S'01–M'04–SM'08–F'15) received the B.S. degree in telecommunications engineering, the M.S. degree in electronics engineering, and the Ph.D. degree in power electronics from the Technical University of Catalonia, Barcelona, in 1997, 2000, and 2003, respectively.

Since 2011, he has been a Full Professor with the Department of Energy Technology, Aalborg University, Denmark, where he is also responsible for the Microgrid Research Program. Since 2014, he has been the Chair Professor with Shandong University. Since 2015, he has been a Distinguished Guest Professor with Hunan University. Since 2016, he has been a Visiting Professor Fellow with Aston University, U.K., and a Guest Professor with the Nanjing University of Posts and Telecommunications. He has published more than 500 journal papers in the fields of microgrids and renewable energy systems, which are cited more than 30 000 times. His research interests include different microgrid aspects, including power electronics, distributed energy-storage systems, hierarchical and cooperative control, energy management systems, smart metering and the Internet of Things for AC/DC microgrid clusters, and islanded minigrids, recently specially focused on maritime microgrids for electrical ships, vessels, ferries, and seaports. He received the Best Paper Award of the IEEE TRANSACTIONS ON ENERGY CONVERSION for the period 2014–2015 and the Best Paper Prize of the IEEE-PES, in 2015. He also received the Best Paper Award of the *Journal of Power Electronics*, in 2016. During five consecutive years, from 2014 to 2018, he was named Highly Cited Researcher by the Clarivate Analytics (formerly Thomson Reuters). In 2015, he was elevated as an IEEE Fellow for his contributions on distributed power systems and microgrids. He is also an Associate Editor for a number of IEEE TRANSACTIONS.